Applied Energy 329 (2023) 120235

Contents lists available at ScienceDirect

Applied Energy

journal homepage: www.elsevier.com/locate/apenergy

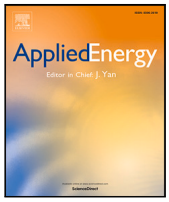

# Fast capacity and internal resistance estimation method for second-life batteries from electric vehicles

Elisa Braco, Idoia San Martín, Pablo Sanchis, Alfredo Ursúa *

*Institute of Smart Cities (ISC), Department of Electrical, Electronic and Communications Engineering, Public University of Navarre (UPNA), Campus de Arrosadía, 31006, Pamplona, Spain*

ARTICLE INFO

*Keywords:*
Energy storage
Electric vehicle
Lithium-ion battery
Second-life battery
Characterization

ABSTRACT

The success of second-life (SL) Li-ion batteries from electric vehicles is still conditioned by their technical and economic viability. The knowledge of the internal parameters of retired batteries at the repurposing stage is key to ensure their adequate operation and to enlarge SL lifetime. However, traditional characterization methods require long testing times and specific equipment, which result in high costs that may jeopardize the economic viability of SL. In the seek of optimizing the repurposing stage, this contribution proposes a novel fast characterization method that allows to estimate capacity and internal resistance at various state of charge for reused cells, modules and battery packs. Three estimation models are proposed. The first of them is based on measurements of AC resistance, the second on DC resistance and the third combines both resistance types. These models are validated in 506 cells, 203 modules and 3 battery packs from different Nissan Leaf vehicles. The results achieved are satisfactory, with mean absolute percentage errors (MAPE) below 2.5% at cell and module level in capacity prediction and lower than 2.4% in resistance estimation. Considering battery pack level, MAPE is below 4.2% and 1.8% in capacity and resistance estimation respectively. With the proposed method, testing times are reduced from more than one day to 2 min per cell, while energy consumption is lowered from 1.4 kWh to 1 Wh. In short, this study contributes to the reduction of repurposing procedures and costs, and ultimately to the success of SL batteries business model.

## 1. Introduction

Nowadays, the transition of the automotive sector towards electric vehicle (EV) is already a fact. Environmental problems related to traditional internal combustion vehicles, together with government actions and citizen awareness have contributed to the expansion of EVs on our roads, which is expected to hit 145 million units by 2030 [1]. As a result, the demand of Li-ion batteries (LIB) for EVs is forecast at 1239 GWh by 2030 [2].

As a consequence of usage, capacity and power capabilities of LIB fade, which eventually compromise their performance in EVs. Automotive standards set therefore a 20–30% of capacity fade as withdrawal point for LIB in EVs. In recent years, the reuse of these batteries has emerged as an alternative to direct recycling, thereby enlarging their lifetime and representing a beneficial solution from an economic and environmental viewpoint [3]. Stationary applications such as residential photovoltaic installations, less demanding than EVs in terms of performance and energy and power density, are regarded as promising alternatives for these second-life (SL) batteries [4]. The outlook for SL LIB market stands at 26 GWh by 2025 [2], yet its success depends on technical and economic viability.

On the one hand, technical viability of SL batteries is almost a reality nowadays. The reuse of EV LIB can be carried out at three levels: battery pack, module and cell. The selection among them depends on the specific energy requirements of the SL applications, as well as on the related costs, and nowadays several approaches can be found. At industrial level, automotive companies such as Nissan [5], BMW [6] o Daimler [7] have already partnered with energy firms in the constructions of large-scale demonstrators with reused battery packs from EVs. Moreover, commercial SL batteries can be found, with battery packs directly reused [8,9] or reconfigured batteries from SL modules [10,11]. Research contributions have also assessed the viability of SL battery packs, in applications with high power requirements such as frequency regulation [12], or high energy demand such as energy time shifting and demand side management at residential level [13,14]. Performance [15,16] and durability [17] of SL modules have also already been assessed. Nevertheless, the economic viability of reused LIB is still uncertain, with threats as their final cost or price competitiveness of new batteries [18]. Moreover, the standards and regulation specific for reused batteries are scarce. Only UL 1974 is

* Corresponding author.
*E-mail address:* alfredo.ursua@unavarra.es (A. Ursúa).

https://doi.org/10.1016/j.apenergy.2022.120235
Received 3 May 2022; Received in revised form 20 October 2022; Accepted 25 October 2022
Available online 8 November 2022

currently available, which focuses on the evaluation of repurposed batteries [19].

The repurposing stage of SL LIB plays a key role in their economic viability, given that it can represent up to 30% of the total costs [20,21]. The direct reuse of battery packs is a priory the most economic option, given its simplicity. Nevertheless, the lack of energy modularity or the internal dispersion of SL modules [16,22,23] are drawbacks that may affect their lifetime [24,25] and therefore its profitability. For its part, module-level reuse overcomes these issues, although the further repurposing processes required increase costs, which may risk economic viability.

Characterization of reused LIB from EVs is essential to ensure an adequate SL operation, being capacity and resistance the internal parameters normally assessed. Traditional characterization methods consists of several hours of testing, with full charge and discharge cycles to obtain capacity, and current pulses or Electrochemical Impedance Spectroscopy (EIS) measurements to measure internal impedance [26]. Despite their accuracy, the time and infrastructure necessary is today a major barrier to decrease costs. Therefore, a major effort is underway to optimize testing procedures. In recent years, the estimation of internal parameters has emerged as an alternative to characterization, which in general requires complex algorithms based on neuronal networks [27–30], support vector machine [27,31,32] or support vector regression [33–35]. However, the principle of these methods differs. Some authors propose incremental capacity curves to estimate capacity [22,31,36–40], which requires high testing times at low current or high data processing [33]. Other estimation methods are based on current pulses [23,27,28,37] or EIS measurements [40–42]. In a second stage, results are extrapolated to a larger data set, thereby estimating the internal parameters. Nevertheless, the easiness and low number of samples required on the characterization tests are usually in counterbalance with the complexity of the algorithms required.

Considering SL LIB, only few contributions targeting this issue have been found [22,23,27,37,39,41,42]. Given the importance of characterization in SL LIB to ensure economic and technical viability, and the research gap found in easy and quick methods, this work proposes a new approach for the estimation of the internal features that define SL LIB state. More precisely, a method that allows to estimate the internal characteristics that define the state of a battery, i.e., its capacity ($C$) and internal DC resistance ($R_{DC}$), in a quicker and easier procedure than traditional methods is developed. The method is applicable at cell, module and battery pack level, and it can be extrapolated to other battery technologies. The experimental procedure has been carried out with a large sample, covering 506 cells, 203 modules and 3 battery packs, all of them retired from real EVs. The work is organized as follows: Section 2 describes the method developed for the quick estimation of the internal features of the SL cells, modules and battery packs. Section 3 gathers the experimental procedure followed, together with a description of the LIB used and the test bench. The experimental results supporting the proposed method for fast characterization are further discussed in Section 4. The initial analysis lead to the identification of two significant variables for estimation (AC and DC resistances), and as a result three models are proposed, one for each of the significant variables and a third as a combination of both. In addition, this section analyses the influence of the sample size used for model fitting on the accuracy and impact of the proposed method in terms of time and energy consumption. Finally, Section 5 gathers the main conclusions of the work.

## 2. Methodology

The proposed method is divided in two main stages: initial analysis and estimation of variables, as presented in Fig. 1. The starting point of the method is a data set (Data Set 0) of cells, modules or battery packs retired from EVs of a specific chemistry and technology, of size $N_0$. Once the study level is defined, a complete characterization is carried out in a selected sample of Data Set 0 (Sample 0), with size $n_0$. The analysis of results allows to identify the relevant significant variables that show strong correlation with $C$ and $R_{DC}$, as well as to fit the estimation models (Estimation models 0). A fast characterization procedure for measuring these relevant variables is also designed, which allows to optimize resources and testing times. Moreover, the minimum number of samples necessary to get representative results ($n_s$) is analysed. The second stage of the method starts with a Data Set 1 of $N_1$ samples with similar chemistry and technology than Data Set 0. The fast characterization procedure is applied to this batch, which allows to statistically determine whether it is similar to Data Set 0. If so, $C$ and $R_{DC}$ will be assessed by means of Estimation models 0. Otherwise, a complete characterization is performed in $n_s$ samples of Data Set 1 (Sample 1.1), in such a way that the estimation models are adjusted (Estimation models 1). These models will be applied to the remaining samples of Data Set 1 (Sample 1.2), thereby estimating the targeted variables.

### 2.1. Stage 1: initial analysis

The first step of the method focuses on the general analysis of the SL samples. Thereby, from a Data Sample 0, it seeks to select the study level (cell, module or battery pack), to identify the significant variables for $C$ and $R_{DC}$ estimation, and finally to define the fast characterization procedure. Moreover, model fitting is also targeted, together with the definition of the minimum sample size to get representative estimation results ($n_s$).

#### 2.1.1. Selecting the level of the study

EV battery reuse is not a standardized procedure [3], and therefore the repurpose at cell, module or battery pack level is possible. When more than one option is available, i.e., modules and their corresponding cells, it is important to assess which approach is the most suitable. On the one hand, the reuse at module level leads to shorter testing times, but the higher voltage levels required in the measuring equipment could increment final costs. On the other hand, cell repurposing allows more precise management and balancing in SL applications. Besides, the operating conditions of the cells from a given module in an EV may vary due to their position, which may result in dispersion on their internal parameters [16,23]. Characterization at cell level would hence overcome this issue, also representing a cost-effective solution regarding requirements for testing equipment. The selection of the study level, if possible, will hence depend on the interests of the specific case.

#### 2.1.2. Complete characterization and analysis

Once the study level is selected, a random sample (Sample 0) of $n_0$ units is selected from Data Set 0. The reception open circuit voltage ($OCV_0$) is firstly measured, thereby discarding samples out of the safety limits set by the manufacturer. Then, the characterization procedure described in Section 3.2 is carried out. The reuse of too damaged samples should be avoided, given that it may compromise SL reliability and lifetime. Thus, threshold values for the characterization parameters are defined, in such a way that a second screening is performed to remove units which do not meet the requirements. The total population size is kept to $n_0$, so if any sample is removed, new units will be tested to meet this number.

*Significant variables and fast estimation method.* After data screening, the significant variables related to $C$ and $R_{DC}$ are identified. To this end, Pearson correlation coefficient (PCC) is used as indicator, given by Eq. (1).

$$PCC_{X,Y} = \frac{COV(X,Y)}{\sigma_X \sigma_Y} \tag{1}$$

$COV(X,Y)$ is the covariance between the target variables $Y$ ($C$ and $R_{DC}$) and the significant variables $X$, while $\sigma_X$ and $\sigma_Y$ are the standard

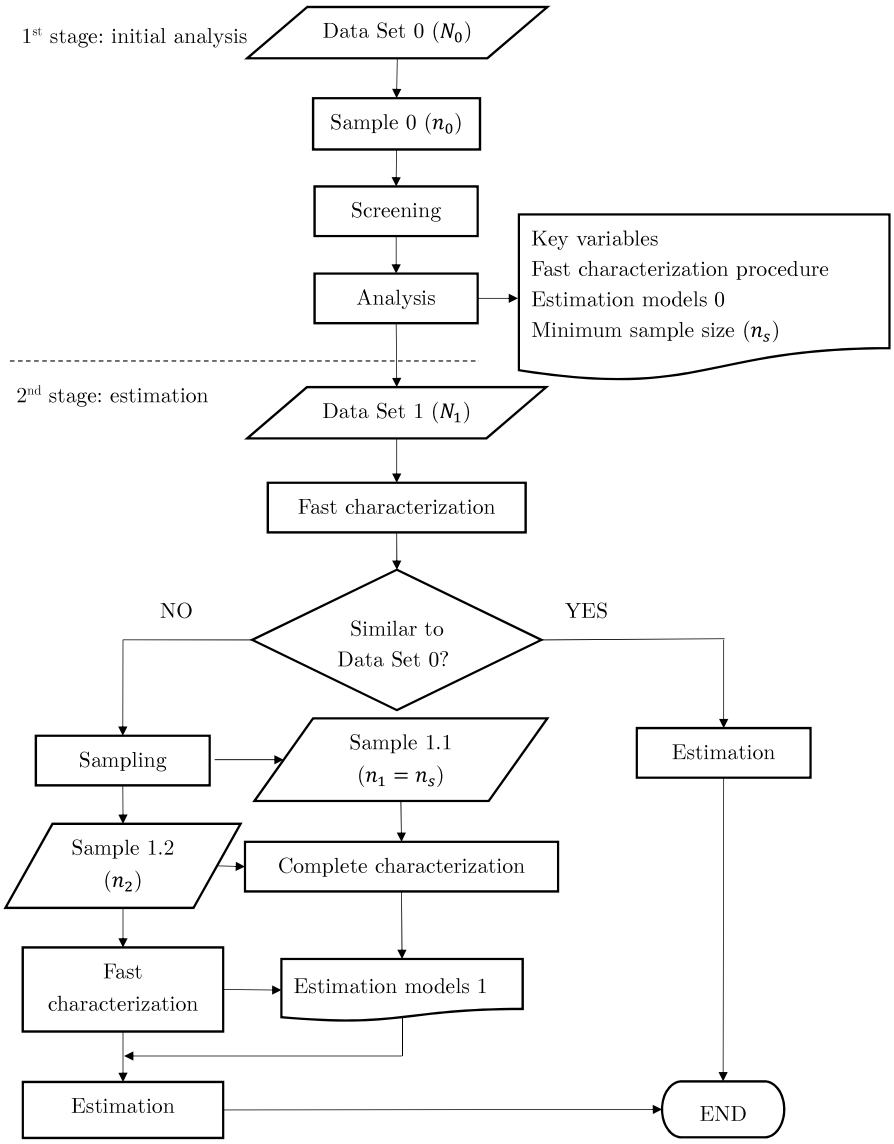


**Fig. 1.** Flowchart of the proposed method for quick estimation of capacity and internal resistance in SL batteries.

deviation of $X$ and $Y$, respectively. The value of $PCC_{X,Y}$ can range from −1 to +1. A value of $PCC_{X,Y}$ of +1 implies a perfect positive linear correlation between $X$ and $Y$, a $PCC_{X,Y}$ of 0 denotes the absence of linear correlation, and a $PCC_{X,Y}$ of −1 implies a perfect negative linear correlation [43]. Moreover, an analysis of variance (ANOVA) test is carried out, with the null hypothesis of no correlation with $X$ and $Y$. If the resulting $P$-value is lower than 0.05, this hypothesis will be rejected with 95% of confidence. Once the significant variables are identified, a fast characterization procedure to obtain them will be designed, aiming to minimize testing times and processes.

*Model fitting.* The general expression for the model relating the target and the significant variables is given by Eq. (2).

$$Y_i = Y_0 + \alpha_1 X_1 + \beta_1 X_2 + \gamma_1 X_3 + \cdots + \alpha_m X_1^m + \beta_m X_2^m + \gamma_m X_3^m \tag{2}$$

The degree and coefficients of each model are fitted with an iterative procedure. Considering a given degree $m$, the assumption of significance for the variable is tested by means of an ANOVA test. If rejected, the procedure is repeated with $m$ equal to the next lower integer, until the degree that considers all the significant terms is found. Then, the resulting polynomial is fitted through least squares method, thereby obtaining Estimation models 0. To evaluate the accuracy of the models, mean absolute percentage error (MAPE) and root mean squared error (RMSE) are computed, according to Eqs. (3) and (4).

$$MAPE\ (\%) = \frac{1}{n}\sum_{i=1}^{n}\frac{|Y_i - \hat{Y}_i|}{Y_i}\cdot 100 \tag{3}$$

$$RMSE = \sqrt{\frac{\sum_{i=1}^{n}(Y_i - \hat{Y}_i)^2}{n}} \tag{4}$$

being $Y$ the measured value, $\hat{Y}$ the estimation and $n$ the size of the sample.

*Influence of sample size on estimation.* When optimizing testing times, the number of samples to be characterized plays a key role. Therefore, the influence of sample size necessary to obtain similar results as in greater populations ($n_s$) is analysed. Relative error is the parameter selected to assess this influence, computed as the absolute value of the difference between the real value and the estimation, divided by the real value. The overall population, with size $N$, has an relative error with given average (MAPE) and standard deviation values. From this population, it is possible to extract n-sized samples, each with its own MAPE, being $n < N$. Statistically, the dispersion of sample averages for different $n$ with respect to the overall population average can be

computed by means of the standard error of the sample mean ($SE$). Eq. (5) shows the calculation of $SE$, adjusted to finite populations.

$$SE = \frac{\sigma}{\sqrt{n}} \cdot \frac{\sqrt{N-n}}{N-1} \quad (5)$$

where $\sigma$ is the standard deviation of MAPE. $N$ is the overall population size and $n$ is the sample size. By computing the derivative of $SE$ over $n$, it is possible to define the minimum sample size from which there is no improvement in estimation ($n_s$).

### 2.2. Stage 2: fast estimation

In this second step, a population with similar chemistry and technology as Data Set 0 is considered, named as Data Set 1 and sized $N_1$. First, the possibility of directly reusing Estimation models 0 is considered, which would be the case if both populations were similar. Otherwise, model adjustment is necessary. To compare both populations, a fast characterization is performed in Data Set 1, from which the values of the significant variables for estimation are obtained. Then, a statistical comparison of the characterization results is performed. The evaluation of differences between data sets depends on their statistical distribution. Hence, a normality test is firstly applied to the fast characterization results of both Data Sets 0 and 1. As widely used solution, Shapiro–Wilk test is recommended. If the set follows a normal distribution, an ANOVA test is performed, as it compares average values. Otherwise, Kruskal–Wallis test is used, given that it targets medians and is recommended when there are outliers. From any of these tests, it is thus possible to statistically compare the sets. These tests probe the hypotheses of equality between the groups, which are rejected with 95% confidence if the resulting $P$-value indicator is lower than 0.05.

Therefore, if Data Set 1 and 0 are similar, Estimation models 0 can be used. Failing that, a random $n_s$-sized sample will be taken from Data Set 1 (Sample 1.1), and a fast characterization will be performed. Note that $n_s$ has been previously defined on Stage 1. From the characterization data, the models will be adjusted (Estimation models 1 in Fig. 1) and applied to the remaining units of Data Set 1 (Sample 1.2).

## 3. Experimental setup

### 3.1. Battery description

The batteries used in this contribution come from different Nissan Leaf EVs. The specific history of their first use, as well as the battery pack of origin are unknown. Each Nissan Leaf battery pack, shown in Fig. 2 is formed by 48 modules in series as the ones depicted in Fig. 2. In turn, each module is formed by four pouch-type cells of LNO/LMO cathode and graphite anode. The cells are connected in pairs associated in series (2s2p). Three external terminals are available in the modules: positive, middle-point and negative, in such a way that 2p cells is the smallest testing unit [17]. This 2p cells will be hereinafter named as "cell" to ease reading. Therefore, Cell-SUP refers to cells between the positive and middle-point terminals, and Cell-INF between the middle and negative ones. The main specifications of battery pack, module and cell are gathered in Table 1.

### 3.2. Experimental procedure

The experimental procedure of this contribution focuses on the characterization of retired batteries from EVs. As previously mentioned, two types of characterization can be distinguished: fast and complete.

The fast characterization consists of three measurements: initial open circuit voltage ($OCV_0$), AC internal resistance ($R_{AC}$) and DC initial resistance ($R_{DC,0}$). These measurements are performed at ambient laboratory temperature (23 ± 2 °C) and with the battery at rest. First, $OCV_0$ between battery terminals is measured. On a second stage, $R_{AC}$ is measured by means of an AC current at 1 kHz. Finally, $R_{DC,0}$ is obtained from a discharge pulse at C/2 during 30 s, considering the initial voltage and current ($V_0$ and $I_0$) and their homologues after 10 s ($V_2$ and $I_2$), computed as $R_{DC,0} = (V_2 - V_0)/(I_2 - I_0)$. C is defined according to the rated capacity of the cell shown in Table 1.

The complete characterization procedure is based on a capacity and resistance measurement at different state of charge ($SOC$) levels. It is performed at a controlled temperature of 25 ± 1 °C in cells and at a laboratory ambient temperature of 23 ± 2 °C in battery packs. The capacity test starts with a 2 h rest period, so that the battery reaches thermodynamic equilibrium. Then, three full cycles at C/3 are performed between the voltage limits. Charge is performed in two steps: constant current and constant voltage (CC-CV), with a cut-off current of C/30 in the CV phase. The capacity of the battery is defined according to the value obtained in the third discharge cycle. Then, the battery is fully charged at C/2 and discharged with the same rate until 90% of SOC. After a 1-h rest, voltage and current are kept ($V_1$ and $I_1$), and a CC discharge pulse at C/2 is performed until the next SOC level. The values of voltage and current after 10 s are also tracked ($V_2$ and $I_2$), and $R_{DC}$ is computed as $R_{DC} = (V_2 - V_1)/(I_2 - I_1)$. This procedure is repeated at 90%, 70%, 30% and 10%. Fig. 3 shows voltage (blue lined) and current (red line) of the $C$ and $R_{DC}$ measurements in a cell.

Moreover, in order to determine the relationship between $OCV$ and $SOC$, a quasi-OCV test is performed. From a fully charged cell, after a 2-h rest period it is CC discharged at C/30 until the lower voltage limit. Then, after a 2-h rest the cell is CC charged with the same rate. This test is also performed at controlled ambient temperature of 25 ± 1 °C. The OCV–SOC curve is computed from the average value of charge and discharge voltages.

### 3.3. Test bench

Fig. 2 shows the test bench used in this contribution. Three multichannel battery testers standing 5 V and 50 A per channel are used, which have a measurement precision of ±0.1% of their full scale. Moreover, two climatic chambers, ranging −30 °C to +180 °C and with a precision of ±0.5 °C are used. On the other hand, the bench also has a battery pack tester of 800 V and 90 A, accurate up to ±0.1% of its full scale. $R_{AC}$ measurement at 1 kHz are performed with a battery analyser with 0.001 mΩ, which stands 60 V and 100 mA, and has a precision of ±1% of its full scale. $OCV$ is measured by means of a multimeter with 0.1 mV resolution. Data processing and statistical analysis are carried out with Matlab R2020a and StatGraphics 18-X64 software.

## 4. Results and discussion

### 4.1. Initial analysis

The first stage of the proposed method is the selection of the study level. As described in Section 3.2, the Nissan Leaf modules analysed have a 2s2p configuration with their Cell-SUP and Cell-INF available. The initial analysis is carried out at cell level, and Cell-SUP are selected as Data Set 0.

As starting point, a Sample 0 of $n_0 = 100$ cells is taken from Data Set 0. First, $OCV_0$ is measured and screened, being all the values tracked within safety limits. Then, $R_{AC}$, $R_{DC,0}$ and $R_{DC}$ are measured according to the procedure described in Section 3.2. To get the receiving $SOC$ of the cells ($SOC_0$), $OCV_0$ measurements and the SOC-OCV curve are used. Even though this curve varies with aging, its changes are minor and can be mostly neglected [44]. Hence, a single curve will be used as representative for the repurposing stage, obtained from the quasi-OCV test performed in one cell with $C$ similar to the average value of Data Set 0. Table 2 shows the statistical resume of the characterization from Sample 0, with average (Avg), standard deviation (Std), maximum (Max), minimum (Min) and coefficient of variation ($CV = Std/Avg$). $OCV_0$ is replaced by the corresponding $SOC_0$, and

**Table 1**
Battery pack, module, and cell specification of Nissan Leaf EV.

| | Battery pack | Module | Cell |
|---|---|---|---|
| Nominal voltage (V) | 360 | 7.50 | 3.75 |
| Maximum voltage (V) | 403.2 | 8.30 | 4.15 |
| Minimum voltage (V) | 240 | 5.0 | 2.5 |
| Rated capacity (Ah) | 66.2 | 66 | 66 |
| Rated energy (Wh) | 24,000 | 495.0 | 247.5 |
| Rated $R_{DC,50\%}$ (mΩ) | 93.1 | 1.94 | 0.970 |
| Rated $R_{AC}$ (mΩ) | 59.8 | 1.25 | 0.623 |
| Length × Width × Thickness (mm) | 1570.5 × 1188.0 × 264.9 | 303 × 223 × 35 | – |
| Mass (kg) | 293 | 3.85 | 1.57 |

**Table 2**
Characterization results of Sample 0.

| | $R_{AC}$ (p.u.) | $SOC_0$ (%) | $R_{DC,0}$ (p.u.) | $C$ (p.u.) | $R_{DC,90\%}$ (p.u.) | $R_{DC,70\%}$ (p.u.) | $R_{DC,50\%}$ (p.u.) | $R_{DC,30\%}$ (p.u.) | $R_{DC,10\%}$ (p.u.) |
|---|---|---|---|---|---|---|---|---|---|
| Avg | 2.02 | 36.2 | 2.20 | 0.66 | 2.13 | 2.08 | 2.14 | 2.13 | 2.37 |
| Std | 0.26 | 5.6 | 0.28 | 0.07 | 0.27 | 0.26 | 0.28 | 0.27 | 0.30 |
| Max | 2.42 | 74.3 | 2.61 | 0.95 | 2.56 | 2.46 | 2.54 | 2.54 | 2.87 |
| Min | 0.99 | 11.2 | 1.13 | 0.57 | 1.08 | 1.07 | 1.06 | 1.10 | 1.26 |
| CV (%) | 13.06 | 15.5 | 12.77 | 11.18 | 12.97 | 12.63 | 13.16 | 12.84 | 12.68 |

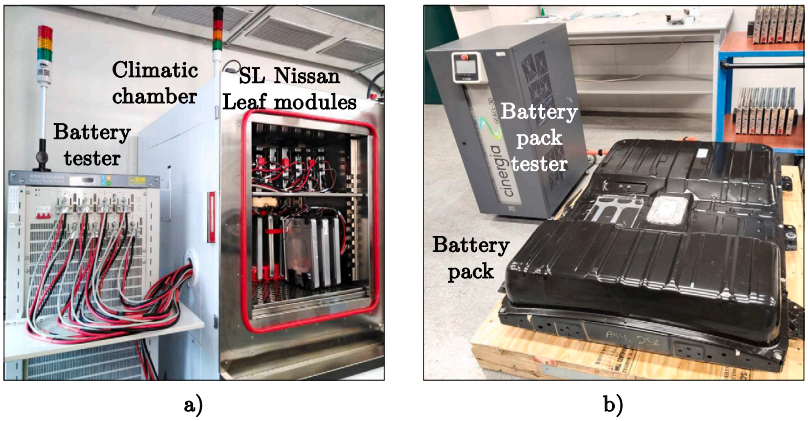


**Fig. 2.** (a) SL Nissan Leaf modules, battery tester and climatic chamber, and (b) Nissan Leaf battery pack and battery pack tester from the test bench.

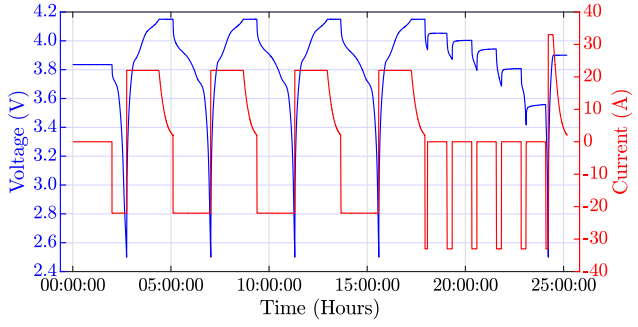


**Fig. 3.** Voltage and current measurements in a cell during a capacity and DC resistance tests in a complete characterization.

the rest of results are normalized with respect to the rated values from Table 1. $R_{DC}$ is shown at the corresponding $SOC$, in such a way that for example $R_{DC,30\%}$ is the measurement performed at 30% of $SOC$.

As can be seen, the normalized value of $C$ ranges from 0.57 to 0.95, with an average of 0.66, slightly lower to the automotive withdrawal limit. Regarding DC resistance, the maximum, minimum and average values of $R_{DC,0}$ are greater than the ones with the closest $SOC$ ($R_{DC,30\%}$) for similar CV. This could be due to the fact that $R_{DC,0}$ is measured after a long rest period in the cell, of several weeks or even months, while $R_{DC}$ test is carried out after several cycles, which promotes the internal kinetics of the cells and as a consequence reduces their internal resistance. On the other hand, it is observed that the maximum average value of $R_{DC}$ is measured at 10% of $SOC$, which is in good agreement with literature [27]. The minimum average value is obtained at a $SOC$ value of 70%.

When it comes to define threshold values for reusable cells, previous degradation tests with similar cells are considered [17], and therefore 0.55 is selected for the normalized $C$ and 4 for normalized $R_{DC}$ and $R_{AC}$ respectively. None of the measurements of Sample 0 reaches the threshold, so all the cells are considered as valid for the analysis.

*Identification of significant variables for fast estimation.* Three candidate variables are considered to be significant for $C$ and $R_{DC}$ estimation: $R_{AC}$, $R_{DC,0}$ and $OCV_0$. From the experimental results of the characterization in Data Set 0, PCC and the $P$-value of the ANOVA test are computed, being the results presented in Table 3. To evaluate resistance estimation, the values measured at 50% of $SOC$ are considered. On the other hand, considering DC resistance as candidate for significant variables, the values obtained at 30% of $SOC$ will be analysed, given that it is the closest value to the average reception $SOC$ in Sample 0. As can be seen, PCC shows a high correlation in both capacity and resistance with $R_{AC}$ and $R_{DC,30\%}$, while $OCV_0$ is quantified as weakly related. ANOVA only accepts the hypothesis of no correlation with the same variable. Therefore, it is concluded that the significant variables for $C$ and $R_{DC}$ estimation are $R_{AC}$ and $R_{DC,30\%}$.

Once the significant variables are identified, the fast characterization procedure is defined. $OCV_0$ measurement is kept as screening procedure to discard damaged samples and to determine $SOC_0$. Secondly, $R_{AC}$ is measured as described in Section 3.2. To define $R_{DC}$

**Table 3**
Correlation results between measured variables ($R_{AC}$, $R_{DC,30\%}$ and $OCV_0$) and capacity and internal resistance ($C$ and $R_{DC}$).

| Parameter | Count | C | | $R_{DC}$ | |
|---|---|---|---|---|---|
| | | PCC | *P*-value | PCC | *P*-value |
| $R_{AC}$ | 100 | −0.927 | 0.000 | 0.900 | 0.000 |
| $R_{DC,30\%}$ | 100 | −0.945 | 0.000 | 0.997 | 0.000 |
| $OCV_0$ | 100 | 0.070 | 0.487 | −0.062 | 0.542 |

**Table 4**
Weighting factors for $R_{DC,0}$ and $R_{DC,30\%}$ to be used as input in the estimation models for Data Sample 0.

| SOC (%) | 10 | 30 | 50 | 70 | 90 |
|---|---|---|---|---|---|
| $F_{SOC}$ | 0.8979 | – | 0.9925 | 1.0226 | 0.9985 |
| $F_0$ | 1.0127 | 0.9670 | 0.9766 | 0.9880 | 0.9880 |

measurement, it is important to note that whereas $R_{AC}$ is independent of $SOC$ [45], $R_{DC}$ varies at high or low levels [26]. The lack of SL standards leads to random $SOC$ at the repurposing stage, even with extreme values [44]. Thereby, it is proposed to adjust the $R_{DC,0}$ measurement of an initial step to a fixed $SOC$, in order to get the input values for the model. More precisely, 30% is selected, given that it is the closest to the average $SOC_0$ of Sample 0. The weighting factors are determined from experimental measurements.

On the one hand, the influence of $SOC_0$ is taken into account by a factor $F_{SOC}$, which considers the ratio between the average resistance values from the characterization test at 30% ($\overline{R_{DC,30\%}}$) and the average values of resistance at the $SOC$ closest to the reception ($\overline{R_{DC,SOC_0}}$), as given by Eq. (6).

$$F_{SOC} = \frac{\overline{R_{DC,30\%}}}{\overline{R_{DC,SOC_0}}} \tag{6}$$

On the other hand, the resistance of a cell after a long inactivity period may be higher than its real value after being cycled [46], which could compromise the accuracy of the estimation methods. Therefore, from the average experimental values after this initial step ($\overline{R_{DC,0}}$) and the ones obtained from the characterization test at a $SOC$ of 30% ($\overline{R_{DC,30\%}}$), a weighting factor $F_0$, is defined according to Eq. (7).

$$Fo = \frac{\overline{R_{DC,30\%}}}{\overline{R_{DC,0}} \cdot F_{SOC}} \tag{7}$$

Table 4 gathers the values of $F_{SOC}$ and $F_0$ considering the experimental results of Data Sample 0, and using Eqs. (6) and (7) for the five $SOC$ levels tested. As can be seen, $F_{SOC}$ shows similar average values except at 10%. This could be explained by the lower number of available gaps for Li ions at low $SOC$, which increases the internal resistance [26]. On the other hand, considering $F_0$, there were no samples received at 90% in Data Set 0, so the closest value, i.e. 70% is taken. This provisional value will be substituted if in future complete characterizations there are samples at the corresponding $SOC$.

The average error between the original measurements of $R_{DC,0}$ and $R_{DC,30\%}$ is 3.4%, while after applying the weighting factors it decreases to 0.1%. The maximum error also decreases from 13.2% to 5.4%. It can be therefore concluded that the factors proposed for Data Sample 0 allow to mitigate the heterogeneity of $R_{DC,0}$.

*Fast estimation models fitting.* In the previous step, two significant variables for the estimation of $C$ and $R_{DC}$ were identified: $R_{AC}$ and $R_{DC,30\%}$. Considering Eq. (2), three models can be thereby fitted with the results of the characterization tests. More precisely, $R_{AC}$ is taken as $X_1$, while $R_{DC,30\%}$ is $X_2$. Based on the procedure described in Section 2.1.2, the degree and coefficients for each model are found. Table 5 shows the best fitting and coefficients for the models in Data Sample 0. The accuracy of the models is evaluated by means of the coefficient of determination (Rsq). Note that when $R_{DC,30\%}$ itself is targeted for estimation, only Model 1 can be used.

To sum up, three estimation models are available, one for each significant variable and a third combining both. When it comes to model fitting, $C$ shows a second-degree correlation with $R_{AC}$ and $R_{DC,30\%}$ with better fitting in Model 2, which can be justified by the greater correlation found through PCC. On the other hand, $R_{DC}$ is linear with both $R_{AC}$ and $R_{DC,30\%}$, and likewise $R_{DC,30\%}$ shows greater PCC and Rsq. Note that $R_{DC,30\%}$ is the target variable, so it is not considered as input for Models 2 and 3. Considering Model 3, the best fitting is a second-order polynomial for $R_{AC}$ and linear with $R_{DC,30\%}$. The better results obtained in resistance models compared to capacity, can be justified by its greater correlation with the input parameters.

*Sample size for estimation.* The initial analysis considers 100 cells from Sample 0. However, given the importance of optimizing repurposing costs and times, the influence of sample size on the estimation is assessed. The aim is thus to define the minimum sample size $n_s$ to obtain similar accuracy results in the models as the ones obtained. To this end, $SE$ in Sample 0 is analysed, according to Eq. (5). The standard deviation of $SE$ in $C$ is 3.8, 2.8 and 2.7 from Model 1, 2, and 3 respectively, while $R_{DC,30\%}$ ranges from 5.6 to 5.8 in Model 1, 0.8 to 1.7 in Model 2 and 0.8 to 1.3 in Model 3. Fig. 4(a) shows the results of the $SE$ in the sample mean depending on the sample size ($n$) for the three capacity models. As can be seen, as $n$ increases the error between sample and overall population mean decreases, which is consistent with the unbiased character of the sample mean [43]. However, the decreasing ratio changes, slowing down as $n$ increases. Fig. 4(b) shows the derivative of $SE$ of the sample mean depending on $n$ for the three estimation models proposed. As the figure shows, from a given value of $n$ there is almost no variation in $SE$, which will be selected as $n_s$. Considering the results from Data Sample 0, the values selected for $dSE/dn$ in $C$ and $R_{DC}$ are 1e−03 and 1.5e−03 respectively, given the greater measurement variability of this second parameter. Hence, the value that meets the requirements for the three models is $n_s$ = 40 in both $C$ and $R_{DC}$.

### 4.2. Fast estimation

Once the initial analysis is carried out, the second stage of the method focuses on the fast estimation of $C$ and $R_{DC}$, which will be carried out at cell, module and battery pack level.

#### 4.2.1. Cells

In order to compare different scenarios, two data sets of cells are considered, with the same chemistry and technology of Sample 0.

- Data Set A: formed by 103 cells ($N_A$) of type Cell-SUP from a different batch than Data Set 0.
- Data Set B: consisting of 203 cells ($N_B$) of type Cell-INF.

Firstly, both data sets are characterized according to the fast procedure defined in Section 3.2. Table 6 shows the statistical resume of the experimental results obtained, with $R_{AC}$ and $R_{DC,0}$ normalized considering their rated values of Table 1. As can be seen, resistance values are greater in Data Set B. Given that the only distinctive feature between both data sets is the position in the module, this fact confirms that EV usage leads to different degradation rates in the cells, specially affecting the ones placed between the middle and negative terminals. This is in good agreement with previous experimental contributions carried out with similar modules [16]. It should be also highlighted the larger $SOC$ variability observed in Data Set B, three times greater than Data Set A, which, together with the high values of $SOC_0$ reported, up to 98%, confirm the need to adapt $R_{DC,0}$ to a fixed $SOC$ value in order to reduce this variations.

Following the method, the data sets are compared to Data Set 0 to determine their similarity. First, a normality test is applied to the fast

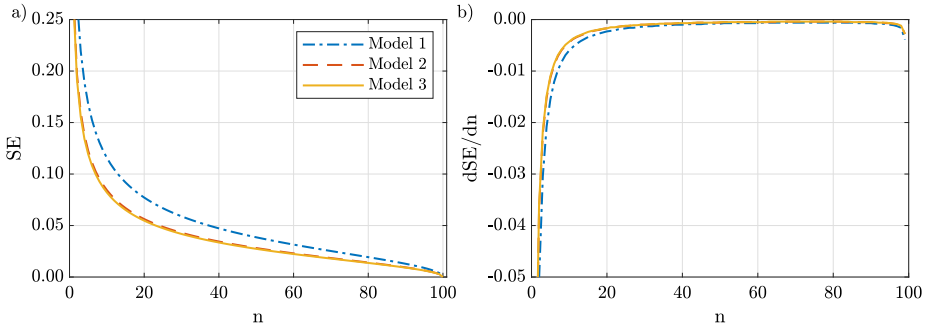


**Fig. 4.** (a) Standard error ($SE$) of the sample mean and (b) its derivative depending on sample size $n$ for the capacity estimation from the three models proposed for Sample 0.

**Table 5**
Coefficients and Rsq for the best fitting of capacity and internal resistance estimation models based on $R_{AC}$ (Model 1), $R_{DC,30\%}$ (Model 2) and both parameters (Model 3) obtained in Data Set 0.

| Model | $X_i$ | $Y$ | $Y_o$ | $\alpha_1$ | $\alpha_2$ | $\beta_1$ | $\beta_2$ | Rsq |
|---|---|---|---|---|---|---|---|---|
| 1 | $R_{AC}$ | $C$ | 1.4602 | −0.6149 | 0.1058 | – | – | 0.888 |
| | | $R_{DC,90\%}$ | 0.2407 | 0.9352 | – | – | – | 0.795 |
| | | $R_{DC,70\%}$ | 0.2816 | 0.8903 | – | – | – | 0.795 |
| | | $R_{DC,50\%}$ | 0.1985 | 0.9626 | – | – | – | 0.807 |
| | | $R_{DC,30\%}$ | 0.2549 | 0.9267 | – | – | – | 0.799 |
| | | $R_{DC,10\%}$ | 0.3374 | 1.0052 | – | – | – | 0.777 |
| 2 | $R_{DC,30\%}$ | $C$ | 1.5887 | – | – | −0.6952 | 0.1187 | 0.937 |
| | | $R_{DC,90\%}$ | −0.0189 | – | – | 1.0102 | – | 0.996 |
| | | $R_{DC,70\%}$ | 0.0372 | – | – | 0.9605 | – | 0.996 |
| | | $R_{DC,50\%}$ | −0.0500 | – | – | 1.0311 | – | 0.995 |
| | | $R_{DC,30\%}$ | – | – | – | – | – | – |
| | | $R_{DC,10\%}$ | 0.0456 | – | – | 1.0919 | – | 0.985 |
| 3 | $R_{AC}$ | $C$ | 1.4311 | −0.4016 | −0.1412 | 0.0814 | – | 0.942 |
| | $R_{DC,30\%}$ | $R_{DC,90\%}$ | −0.0131 | −0.0117 | 0.0018 | 1.0150 | – | 0.996 |
| | | $R_{DC,70\%}$ | −0.0526 | 0.1218 | −0.0342 | 0.9538 | – | 0.961 |
| | | $R_{DC,50\%}$ | −0.2291 | 0.2682 | −0.0659 | 0.9891 | – | 0.996 |
| | | $R_{DC,30\%}$ | – | – | – | – | – | – |
| | | $R_{DC,10\%}$ | 0.4991 | −0.6366 | 0.1707 | 1.1501 | – | 0.989 |

**Table 6**
Statistical resume of the fast characterization results of Data Set A and B.

| | $R_{AC}$ | | $SOC_0$ (%) | | $R_{DC,0}$ | |
|---|---|---|---|---|---|---|
| | A | B | A | B | A | B |
| Mean | 1.99 | 2.11 | 36.1 | 39.2 | 2.17 | 2.38 |
| Std | 0.40 | 0.32 | 3.8 | 13.3 | 0.38 | 0.39 |
| Max | 2.70 | 2.71 | 50.4 | 98.1 | 2.69 | 2.96 |
| Min | 0.98 | 1.16 | 11.1 | 10.9 | 1.20 | 1.19 |
| CV (%) | 20.01 | 15.24 | 10.6 | 34.0 | 17.34 | 16.90 |

characterization results, concluding that none of the variables follow a normal distribution. This is consistent with other research works that analyse statistically SL batteries from EVs [22]. After applying Kruskal–Wallis method, P-values of 0.32 and 0.13 are obtained for $R_{DC,0}$ and $R_{AC}$ in Data Set A, which accept the hypothesis of similarity with Data Set 0. Therefore, the Estimation models 0 will be used in Data Set A, with the coefficients from Table 5. Nevertheless, in Data Set B the P-values obtained are 0.00, which shows that this population is different from Data Set 0. It is thus necessary to adapt the estimation models to the new data. To do so, a sample of $n_s = 40$ cells will be randomly taken from Data Set B. The cells are completely characterized, according to the procedure described in Section 3.2. The estimation models are then fitted, and the new factors and coefficients obtained. Using these adjusted models (Estimation models 1 in Fig. 1), $C$ and $R_{DC}$ are estimated in the remaining cells of Data Set B.

Fig. 5(a) and (b) show the experimental results of capacity and internal resistance measured at the five SOC levels in the complete characterization test. These values are compared to the estimations with the proposed methodology, being the accuracy results of $C$ and $R_{DC}$ estimation in Data Sets A and B presented in terms of RMSE and MAPE in Fig. 5(c) and (d) respectively. To consider all the cells and decrease the influence of sampling, models are trained and tested by means of cross-validation. 5 folds are considered, so that the requirement of $n_s = 40$ for training is kept. The results shown in Fig. 5 are the average value of the 5 trials.

As can be seen, in general $C$ shows better accuracy results, which could be expected given the greater magnitude and lower variability of this parameter. Model 3 has the best results, with RMSE of 1.9% and 2.0% in Data Sets A and B, and MAPE of 2.3% and 2.5% respectively. Considering, $R_{DC}$, the best estimation leads to RMSE of 4.3% in Data Set A and 6.8% in B, while MAPE is 2.2% and 2.4% on each set, respectively. Compared to other contributions that target SL characterization at the repurposing stage, these are generally focused on capacity estimation, with errors below 2% [42], 3% [22,47] or even 5% [23], but considering other input variables such as partial charge [47], partial discharge [23], EIS [42] or incremental capacity [22,23].

#### 4.2.2. Modules

This subsection goes a step further in the estimation of features from SL batteries, by targeting module level. To do so, a Data Set C formed by 203 modules is analysed. The characterization results of this data set are obtained from the experimental measurements of their constituent cells, previously described in this contribution. Hence, in a given module, $C$ is defined as the lowest value of its 2p cell pairs, while $R_{DC}$ is the sum of them. Table 7 shows the statistical resume of the fast characterization in Data Set C, normalized with the rated values of Table 1.

Following the method, a normality test is carried out, which shows that none of the estimation variables follow a normal distribution. Kruskal–Wallis test is then applied, which gives P-values of 0.00 in both

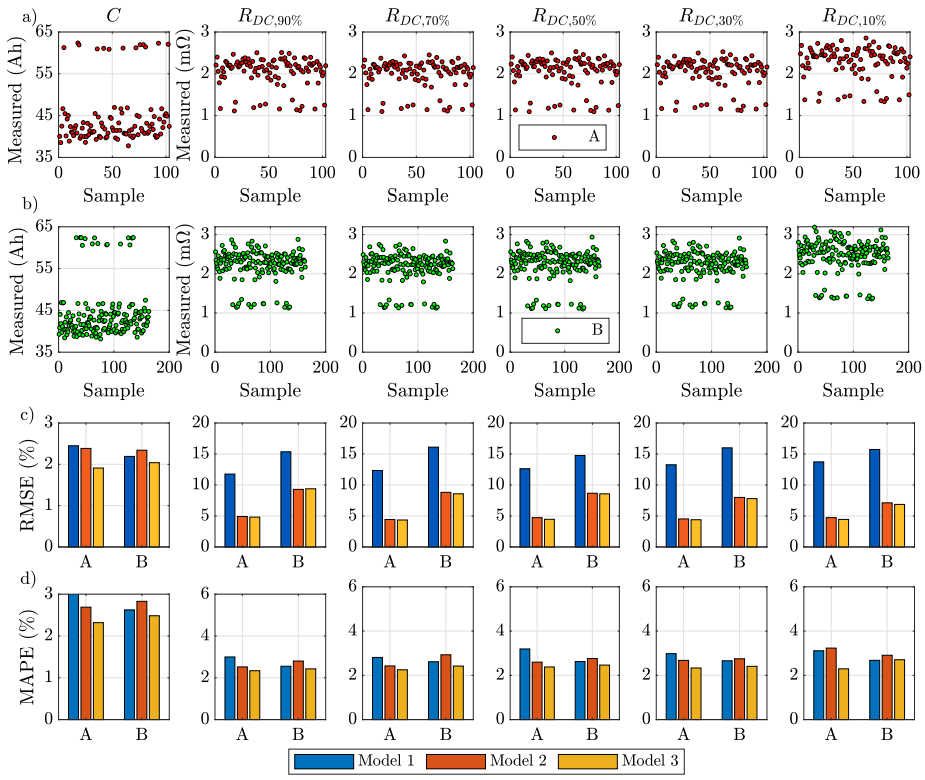


**Fig. 5.** Experimental results of capacity and internal resistance in (a) Data Set A and (b) Data Set B, and accuracy results of estimation in terms of (c) RMSE and (d) MAPE in Data Sets A and B depending on the estimation model.

**Table 7**
Fast characterization results of Data Set C.

| | $R_{AC}$ | $SOC_0$ (%) | $R_{DC,0}$ |
|---|---|---|---|
| Mean | 2.06 | 37.4 | 2.20 |
| Std | 0.41 | 6.7 | 0.68 |
| Max | 2.55 | 62.6 | 2.73 |
| Min | 1.08 | 11.0 | 1.12 |
| CV (%) | 15.73 | 18.0 | 15.85 |

**Table 8**
Fast characterization results of Data Set D.

| Battery pack | $SOC_0$ (%) | $R_{DC,0}$ (mΩ) |
|---|---|---|
| D1 | 79.1 | 129.2 |
| D2 | 23.3 | 126.9 |
| D3 | 40.5 | 205.5 |

values, thereby detecting differences between Data Sets C and 0 and requiring model adjustments. As in Data Set B, a sample of $n_s = 40$ modules is completely characterized, and the factors and coefficients for the models are fitted. $C$ and $R_{DC}$ are estimated in the remaining modules of the data set, with the experimental measurements and accuracy results in terms of RMSE and MAPE shown in Fig. 6(a), (b) and (c), respectively. As in the previous analysis, a cross-validation procedure with 5 folds is followed, in such a way that all the available data is considered in both model training and testing. Similarly, the results shown are the average of all the trials.

As can be observed, RMSE values are lower in $C$ estimation, similarly than at cell level. In particular, 1.9% was achieved, versus 5.7% obtained in the best case for $R_{DC}$. Nevertheless, MAPE is similar in both variables, with a value of 2.3%.

### 4.2.3. Battery packs

Finally, a Data Set D formed by three battery packs (D1, D2 and D3) is also assessed. Given that there are not enough samples to develop specific models for this level of study, their $C$ and $R_{DC}$ will be estimated from the models used at module level.

Therefore, the three battery packs are characterized according to the fast procedure, being the results presented in Table 8. Given that the voltage range of the battery packs exceeds the limits of the measuring device, $R_{AC}$ cannot be determined. To compare the results obtained with module level, the average value of the 203 samples of Data Set C, shown in Table 7 are extrapolated to battery pack level (48 modules in series), resulting in 204.9 mΩ. As can be seen, the values of $R_{DC,0}$ in the battery packs are lower, with the maximum value measured in D3, thereby suggests a worse degradation state of this sample.

To estimate $C$ and $R_{DC}$ with the available data, Model 2 from Section 4.2.2 and the corresponding factors are used. To adapt the measured data, $R_{DC,0}$ from D1, D2 and D3 are divided by the number of modules that form the battery pack, thereby obtaining the equivalent input for the model. Fig. 7 shows the experimental measurements of (a) $C$ and (b) $R_{DC}$ at the five SOC levels, which are compared to the estimated values and with the resulting relative errors of $C$ and $R_{DC}$ estimation obtained on each battery pack plotted in Fig. 7(c) and (d).

As can be seen, relative errors in $C$ range from 2.0% (D2) to 6.6% (D3), resulting in a MAPE of 2.8%. The outliered estimation error in D3 could be explained by its greatest $R_{DC,0}$, from which a lower value of capacity could be expected. Considering $R_{DC}$ prediction, the best results are also obtained in D2, with errors below 1% except from $R_{DC,10\%}$. In this case, MAPE ranges from 1.4%, obtained in $R_{DC,70\%}$ to 8.2% reported in $R_{DC,10\%}$.

### 4.3. Influence of sample size on accuracy

The fast characterization method proposed aims to obtain sufficient data to estimate $C$ and $R_{DC}$ in the remaining units of a given set. Thereby, the size of this sample to be fully characterized ($n_s$) should balance testing times and accuracy. It is hence interesting to analyse

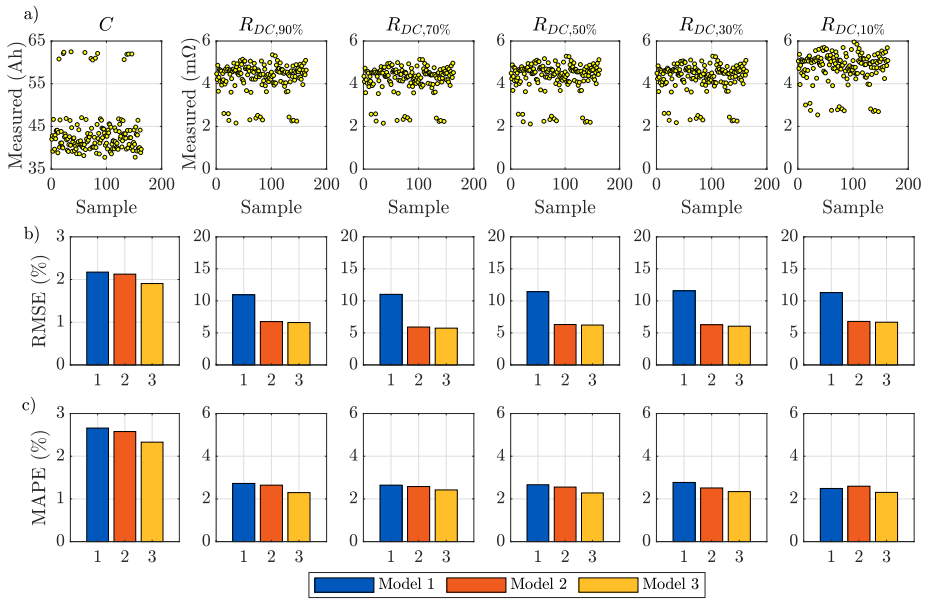


**Fig. 6.** (a) Experimental results of capacity and internal resistance in Data Set C and accuracy results of estimation in terms of (b) RMSE and (c) MAPE depending on the estimation model.

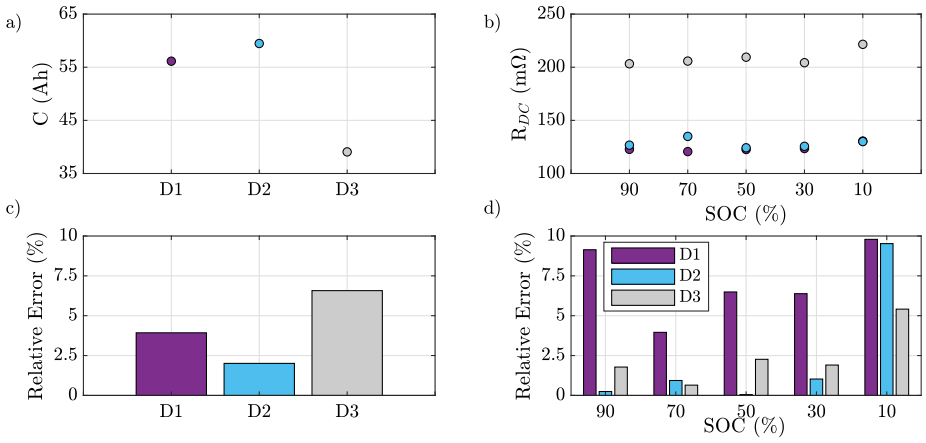


**Fig. 7.** Experimental results of (a) capacity and (b) internal resistance in Data Set D and absolute error in estimation of (c) $C$ and (d) $R_{DC}$ at the different $SOC$ for the three battery packs tested.

how the estimation accuracy varies depending on this parameter. As an illustrative example, Data Set B, formed by 203 cells will be assessed. Therefore, from the experimental results obtained in this set, presented in Section 4.2.1, the value of $n_s$ is varied from 5 to 100, fitting on each case the corresponding estimation models and applying them to estimate the remaining samples. On each case, cross-validation is applied in model testing and training, in such a way that the number of folds is adjusted to meet the corresponding $n_s$. Then, RMSE and MAPE are computed with Eqs. (4) and (3). Fig. 8 shows the resulting evolution of RMSE (Fig. 8a) and MAPE (Fig. 8b) in capacity estimation of Data Set B depending on $n_s$. As can be seen, in Model 3 RMSE is below 2% for $n_s$ greater than 30, while MAPE decreases below 2.5% from $n_s = 40$. Hence, $n_s$ could be modified depending on the accuracy desired.

### 4.4. Impact of the proposed method on testing resources

In addition to the precision of the proposed method, another interesting issue to discuss is its impact on testing times and equipment, as well as in the energy consumed. Table 9 shows the results of time and energy required in this contribution for the proposed estimation procedure at cell level, with their equivalent in a complete characterization. The required equipment in both approaches is also shown.

**Table 9**
Time and energy consumed and required equipment for cell characterization according to the traditional method and the proposed fast estimation procedure.

| | Traditional method | | Proposed method | | Equipment |
|---|---|---|---|---|---|
| | Time (min) | Energy (Wh) | Time (min) | Energy (Wh) | |
| $C$ | 836 | 1071 | – | – | Battery tester climatic chamber |
| $R_{DC}$ | 606 | 357 | – | – | Battery tester climatic chamber |
| $R_{DC,0}$ | 1 | 1 | 1 | 1 | Battery tester |
| $R_{AC}$ | 1 | – | 1 | – | Impedance meter |
| TOTAL | 1444 | 1429 | 2 | 1 | |

As can be seen, the proposed fast estimation method leads to a drastic decrease in testing times, from more than one day to 2 min per cell. Specifically, the fast characterization is carried out, consisting of OCV, AC and DC resistance measurements. Yet considering the parallel use of resources, e.g., several channels at the same time, time reduction is even more clear at industrial level, which deals with much greater volumes of SL samples to repurpose. Energy reduction is also very

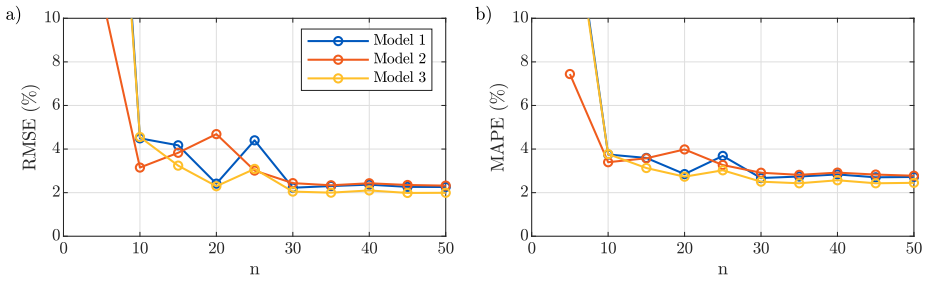


**Fig. 8.** (a) RMSE and (b) MAPE evolution depending on the size of $n_s$ for capacity estimation in Data Set B.

marked, going from 1429 Wh to 1 Wh. The electrical energy consumed when implementing the proposed fast characterization method is approximately 1 Wh, obtained as 33 A × 30/3600 h × 3.75 V = 1.03 Wh. In this case, there are several factors to consider when quantifying advantages, such as the possibility of utilizing the energy obtained from the batteries in the characterization. Regarding the required equipment, it is noteworthy that $R_{DC,0}$ can be measured without a climatic chamber, given that the duration of the current pulse required, of few seconds, is too small to increase the internal temperature of the cells significantly. Therefore, the benefits of the proposed method compared to traditional measurements are demonstrated.

## 5. Conclusion

This contribution proposes a method for the fast estimation of capacity and internal resistance of SL cells, modules and battery packs. The existing need of optimizing characterization procedures at the repurposing stage in order to decrease costs, together with the actual research gap justify the analysis.

The suggested procedure consists of two stages: initial analysis and fast estimation. In the first step, a given data set is characterized, which allows to identify the significant variables for estimation. A fast characterization procedure to measure significant variables is then defined, and the estimation models thus fitted. Moreover, the minimum number of samples to characterize in order to have significant results in the overall population is assessed. In the second stage, a new data set is considered and characterized with the fast procedure. By comparing it statistically to the previous samples, it is possible to determine if they are similar, so that the previous estimation models can be applied. Otherwise, a sample with the minimum number needed is fully characterized, thereby adjusting the models and estimating capacity and resistance in the remaining units.

The proposed method is validated in 506 cells, 203 modules and 3 battery packs, all reused from Nissan Leaf EVs. The significant variables identified for both capacity and resistance estimation are AC and DC resistances. Three estimation models are thereby obtained, one for each target variable and a third combining them. Considering the cells between positive and middle terminal as starting data set, it is statistically demonstrated that the counter-posed cells, between middle and negative terminals, are different, so model adjustment is necessary. Likewise, estimation at module level require new models.

The best accuracy results are obtained by means of the model that combines both AC and DC resistances, with RMSE values below 2% in capacity estimation of cells and modules, and MAPE below 2.5%. In terms of resistance estimation, the average RMSE is lower than 6.4% at cell and module level, while MAPE is below 2.4% in both cases. Considering battery pack estimation, it is only possible to estimate with Model 2 due to equipment limitations, obtaining RMSE values of 3.1% and 7.0% in capacity and resistance, and MAPE below 4.2%. With the proposed method, testing times are reduced from more than one day to 2 min per cell, while energy is reduced from 1.4 kWh to 1 Wh.

Overall, this contribution highlights the importance of optimizing characterization procedures at the repurposing stage of Li-ion batteries from EVs. The assessment of the correlation between the internal variables allows to design a fast characterization procedure and to define estimation models, thereby reducing testing times with good accuracy results. This allows to simplify this stage, thereby reducing its costs and contributing to the economic viability of SL batteries. The proposed method is likely suitable to be adapted to other technologies and chemistries, and such tests are left as future lines of this work.

## CRediT authorship contribution statement

**Elisa Braco:** Conceptualization, Methodology, Software, Formal analysis, Investigation, Visualization, Data curation, Writing – original draft. **Idoia San Martín:** Conceptualization, Methodology, Investigation, Validation, Writing – review & editing. **Pablo Sanchis:** Resources, Supervision, Project administration, Funding acquisition. **Alfredo Ursúa:** Conceptualization, Writing – review & editing, Resources, Supervision, Project administration, Funding acquisition.

## Declaration of competing interest

The authors declare that they have no known competing financial interests or personal relationships that could have appeared to influence the work reported in this paper.

## Data availability

The authors are unable or have chosen not to specify which data has been used.

## Acknowledgements

This work is part of the projects PID2019-111262RB-I00, funded by MCIN/AEI, Spain/10.13039/501100011033/, STARDUST (774094), funded by European Union's Horizon 2020 research and innovation programme, HYBPLANT, Spain (0011-1411-2022-000039), funded by Government of Navarre, Spain, and a Ph.D. scholarship, also funded by Government of Navarre, Spain. Open access funding provided by Universidad Pública de Navarra, Spain.

## References

[1] International Energy Agency. Global EV outlook 2021. 2021, http://dx.doi.org/10.1787/d394399e-en.
[2] Curry C. Lithium-ion battery costs and market. BNEF; 2017, 5 July 2017.
[3] Hossain E, Murtaugh D, Mody J, Faruque HMR, Haque Sunny MS, Mohammad N. A comprehensive review on second-life batteries: Current state, manufacturing considerations, applications, impacts, barriers amp; potential solutions, business strategies, and policies. IEEE Access 2019;7:73215–52. http://dx.doi.org/10.1109/ACCESS.2019.2917859.
[4] Podias A, Pfrang A, Di Persio F, Kriston A, Bobba S, Mathieux F, Messagie M, Boon-Brett L. Sustainability assessment of second use applications of automotive batteries: Ageing of Li-ion battery cells in automotive and grid-scale applications. World Electr Veh J 2018;9:24. http://dx.doi.org/10.3390/wevj9020024.
[5] Nissan. Second life LEAF batteries to power Amsterdam Aren A.

[6] Gohla-Neudecker B, Bowler M, Mohr S. Battery 2nd life: Leveraging the sustainability potential of EVs and renewable energy grid integration. In: 5th international conference on clean electrical power: renewable energy resources impact, ICCEP 2015. IEEE; 2015, p. 311–8. http://dx.doi.org/10.1109/ICCEP.2015.7177641.

[7] Daimler. World's largest 2nd-use battery storage is starting up. 2016, p. 1–2, URL https://media.daimler.com/marsMediaSite/en/instance/ko/Worlds-largest-2nd-use-battery-storage-is-starting-up.xhtml?oid=13634457.

[8] Nissan, Eaton. Xstorage buildings - eaton nissan energy storage systems for buildings. 2017.

[9] Mercedes-Benz. Mercedes-Benz energy storage. A new dimension of energy management. Tech. rep, 2019.

[10] BeePlanet Factory. BeeBattery home datasheet. 2018, URL http://beeplanetfactory.com/wp-content/uploads/2019/12/190727-Datasheet-BeeBatteryHome-EN.pdf.

[11] SNT. Spiers new energy. URL http://www.spiersnewtechnologies.com/energy-storage.

[12] White C, Thompson B, Swan LG. Repurposed electric vehicle battery performance in second-life electricity grid frequency regulation service. J Energy Storage 2020;28(November 2019):101278. http://dx.doi.org/10.1016/j.est.2020.101278.

[13] Li H, Alsolami M, Yang S, Alsmadi YM, Wang J. Lifetime test design for second-use electric vehicle batteries in residential applications. IEEE Trans Sustain Energy 2017;8(4):1736–46. http://dx.doi.org/10.1109/TSTE.2017.2707565.

[14] Tong SJ, Same A, Kootstra MA, Park JW. Off-grid photovoltaic vehicle charge using second life lithium batteries: An experimental and numerical investigation. Appl Energy 2013;104:740–50. http://dx.doi.org/10.1016/j.apenergy.2012.11.046.

[15] Zhang Y, Li Y, Tao Y, Ye J, Pan A, Li X, Liao Q, Wang Z. Performance assessment of retired EV battery modules for echelon use. Energy 2020;193:116555. http://dx.doi.org/10.1016/j.energy.2019.116555.

[16] Braco E, San Martin I, Berrueta A, Sanchis P, Ursua A. Experimental assessment of first- and second-life electric vehicle batteries: Performance, capacity dispersion, and aging. IEEE Trans Ind Appl 2021;57(4):4107–17. http://dx.doi.org/10.1109/TIA.2021.3075180.

[17] Braco E, San Martín I, Berrueta A, Sanchis P, Ursúa A. Experimental assessment of cycling ageing of lithium-ion second-life batteries from electric vehicles. J Energy Storage 2020;32(July):101695. http://dx.doi.org/10.1016/j.est.2020.101695.

[18] Mathews I, Xu B, He W, Barreto V, Buonassisi T, Peters IM. Technoeconomic model of second-life batteries for utility-scale solar considering calendar and cycle aging. Appl Energy 2020;269(January):115127. http://dx.doi.org/10.1016/j.apenergy.2020.115127.

[19] UL1974 - standard for evaluation for repurposing batteries. Standard, Underwriters Laboratories; 2018.

[20] Alharbi T, Bhattacharya K, Kazerani M. Planning and operation of isolated microgrids based on repurposed electric vehicle batteries. IEEE Trans Ind Inf 2019;15(7):4319–31. http://dx.doi.org/10.1109/TII.2019.2895038.

[21] Neubauer J, Smith K, Wood E, Pesaran A. Identifying and overcoming critical barriers to widespread second use of PEV batteries. Energy Rep 2015;23–62, doi:NREL/TP-5400-63332.

[22] Jiang Y, Jiang J, Zhang C, Zhang W, Gao Y, Guo Q. Recognition of battery aging variations for LiFePO4 batteries in 2nd use applications combining incremental capacity analysis and statistical approaches. J Power Sources 2017;360:180–8. http://dx.doi.org/10.1016/j.jpowsour.2017.06.007.

[23] Ahmeid M, Muhammad M, Lambert S, Attidekou PMZ. A rapid capacity evaluation of retired electric vehicle battery modules using partial discharge test. J Energy Storage 2022;50:104562. http://dx.doi.org/10.1016/j.est.2022.104562.

[24] Gogoana R, Pinson MB, Bazant MZ, Sarma SE. Internal resistance matching for parallel-connected lithium-ion cells and impacts on battery pack cycle life. J Power Sources 2014;252:8–13. http://dx.doi.org/10.1016/j.jpowsour.2013.11.101.

[25] Gong X, Xiong R, Mi CC. Study of the characteristics of battery packs in electric vehicles with parallel-connected lithium-ion battery cells. IEEE Trans Ind Appl 2015;51(2):1872–9. http://dx.doi.org/10.1109/TIA.2014.2345951.

[26] Barai A, Uddin K, Dubarry M, Somerville L, McGordon A, Jennings P, Bloom I. A comparison of methodologies for the non-invasive characterisation of commercial Li-ion cells. Prog Energy Combust Sci 2019;72:1–31. http://dx.doi.org/10.1016/j.pecs.2019.01.001.

[27] Lai X, Qiao D, Zheng Y, Ouyang M, Han X, Zhou L. A rapid screening and regrouping approach based on neural networks for large-scale retired lithium-ion cells in second-use applications. J Cleaner Prod 2019;213:776–91. http://dx.doi.org/10.1016/j.jclepro.2018.12.210.

[28] Zhou P, He Z, Han T, Li X, Lai X, Yan L, Lv T, Xie J, Zheng Y. A rapid classification method of the retired LiCoxNiyMn1xyO2 batteries for electric vehicles. Energy Rep 2020;6:672–83. http://dx.doi.org/10.1016/j.egyr.2020.03.013.

[29] Li Y, Li K, Liu X, Wang Y, Zhang L. Lithium-ion battery capacity estimation — A pruned convolutional neural network approach assisted with transfer learning. Appl Energy 2021;285:116410. http://dx.doi.org/10.1016/j.apenergy.2020.116410.

[30] Ma Y, Yao M, Liu H, Tang Z. State of health estimation and remaining useful life prediction for lithium-ion batteries by improved particle swarm optimization-back propagation neural network. J Energy Storage 2022;52:104750. http://dx.doi.org/10.1016/j.est.2022.104750.

[31] Zhou Z, Duan B, Kang Y, Shang Y, Cui N, Chang L, Zhang C. An efficient screening method for retired lithium-ion batteries based on support vector machine. J Cleaner Prod 2020;267:121882. http://dx.doi.org/10.1016/j.jclepro.2020.121882.

[32] Shu X, Li G, Shen J, Lei Z, Chen Z, Liu Y. A uniform estimation framework for state of health of lithium-ion batteries considering feature extraction and parameters optimization. Energy 2020;204:117957. http://dx.doi.org/10.1016/j.energy.2020.117957.

[33] Zhu Z, Zheng Y, Lai X, Feng X, Li X. A novel fast estimation and regroup method of retired lithium-ion battery cells. Int J Energy Res 2020;44(14):11985–97. http://dx.doi.org/10.1002/er.5847.

[34] Yang D, Wang Y, Pan R, Chen R, Chen Z. State-of-health estimation for the lithium-ion battery based on support vector regression. Appl Energy 2018;227:273–83. http://dx.doi.org/10.1016/j.apenergy.2017.08.096, Transformative Innovations for a Sustainable Future – Part III.

[35] Li X, Yuan C, Wang Z. State of health estimation for Li-ion battery via partial incremental capacity analysis based on support vector regression. Energy 2020;203:117852. http://dx.doi.org/10.1016/j.energy.2020.117852.

[36] Jiang B, Dai H, Wei X. Incremental capacity analysis based adaptive capacity estimation for lithium-ion battery considering charging condition. Appl Energy 2020;269:115074. http://dx.doi.org/10.1016/j.apenergy.2020.115074.

[37] Braco E, San Martin I, Sanchis P, Ursúa A, Stroe D-I. Health indicator selection for state of health estimation of second-life lithium-ion batteries under extended ageing. J Energy Storage 2022;55:105366. http://dx.doi.org/10.1016/j.est.2022.105366.

[38] Li Y, Sheng H, Cheng Y, Stroe D-I, Teodorescu R. State-of-health estimation of lithium-ion batteries based on semi-supervised transfer component analysis. Appl Energy 2020;277:115504. http://dx.doi.org/10.1016/j.apenergy.2020.115504.

[39] Schaltz E, Stroe D-I, Nrregaard K, Ingvardsen LS, Christensen A. Incremental capacity analysis applied on electric vehicles for battery state-of-health estimation. IEEE Trans Ind Appl 2021;57(2):1810–7. http://dx.doi.org/10.1109/TIA.2021.3052454.

[40] Zhang Q, Li X, Zhou C, Zou Y, Du Z, Sun M, Ouyang Y, Yang D, Liao Q. State-of-health estimation of batteries in an energy storage system based on the actual operating parameters. J Power Sources 2021;506:230162. http://dx.doi.org/10.1016/j.jpowsour.2021.230162.

[41] Zhang Q, Li X, Du Z, Liao Q. Aging performance characterization and state-of-health assessment of retired lithium-ion battery modules. J Energy Storage 2021;40(May):102743. http://dx.doi.org/10.1016/j.est.2021.102743.

[42] Luo F, Huang H, Ni L, Li T. Rapid prediction of the state of health of retired power batteries based on electrochemical impedance spectroscopy. J Energy Storage 2021;41(May):102866. http://dx.doi.org/10.1016/j.est.2021.102866.

[43] Ugarte MD, Militino AF, Arnholt A. Probability and statistics with R. 1st ed.. Chapman & Hall/CRC; 2008, p. 728.

[44] Zhou Z, Ran A, Chen S, Zhang X, Wei G, Li B, Kang F, Zhou X, Sun H. A fast screening framework for second-life batteries based on an improved bisecting K-means algorithm combined with fast pulse test. J Energy Storage 2020;31(May):101739. http://dx.doi.org/10.1016/j.est.2020.101739.

[45] Schuster SF, Brand MJ, Campestrini C, Gleissenberger M, Jossen A. Correlation between capacity and impedance of lithium-ion cells during calendar and cycle life. J Power Sources 2016;305:191–9. http://dx.doi.org/10.1016/j.jpowsour.2015.11.096.

[46] Reichert M, Andre D, Rösmann A, Janssen P, Bremes H, Sauer DU. Influence of relaxation time on the lifetime of commercial lithium-ion cells. J Power Sources 2013;239:45–53. http://dx.doi.org/10.1016/j.jpowsour.2013.03.053.

[47] Lai X, Deng C, Li J, Zhu Z, Han X, Zheng Y. Rapid sorting and regrouping of retired lithium-ion battery modules for Echelon utilization based on partial charging curves. IEEE Trans Veh Technol 2021;70(2):1246–54. http://dx.doi.org/10.1109/TVT.2021.3055068.